Available online at www.sciencedirect.com
ScienceDirect
Icarus 192 (2007) 605–622
ICARUS
www.elsevier.com/locate/icarus

Mid-infrared (5–100 μm) reflectance spectra and optical constants of ten phyllosilicate minerals

Timothy D. Glotch [a,*,1], George R. Rossman [b], Oded Aharonson [b]

[a] *Jet Propulsion Laboratory, California Institute of Technology, Pasadena, CA 91125, USA*
[b] *Division of Geological and Planetary Sciences, California Institute of Technology, Pasadena, CA 91125, USA*

Received 19 March 2007; revised 18 June 2007

Available online 15 August 2007

Abstract

We have derived the real and imaginary indices of refraction for 10 phyllosilicate minerals—montmorillonite, beidellite, nontronite, hectorite, saponite, illite, illite–smectite (60/40 interlayered) kaolinite, halloysite, and serpentine—from 100–2000 cm^{-1} (5–100 μm) at 2 cm^{-1} spectral sampling using classical Lorentz–Lorenz dispersion theory. We present the real and imaginary indices and the oscillator parameters with which they were modeled. Use of these optical constants will aid in the modeling of thermal infrared spectra of planets, asteroids, interplanetary and interstellar dust, and protoplanetary disks around nearby stars.

Keywords: Spectroscopy; Infrared observations; Mars; Asteroids, observations; Disks; Interplanetary dust

1. Introduction

Silicates are an important component of the surface of Earth, Mars, and other planets, as well as interplanetary and interstellar dust particles, asteroids, and disks surrounding young stars. Studies using both visible/near-infrared (VNIR) and thermal infrared (TIR) spectroscopy have shown that crystalline, hydrous silicates are important phases in these bodies (Lebofsky, 1978; Barber, 1981; Vilas and Gaffey, 1989; Reach et al., 2003; Poulet et al., 2005; Bibring et al., 2005). An important factor in identifying the components of these materials in TIR spectra is the availability of suitable optical constants that allow modeling of scattering, transmission and absorption processes that affect the spectra. Here, we present the estimated optical constants of 10 hydrated phyllosilicates from 100–2000 cm^{-1} (5–100 μm) which were determined by applying classical Lorentz–Lorenz dispersion analysis to high-quality laboratory reflectance spectra.

* Corresponding author. Fax: +1 (631) 632 8240.
E-mail address: tglotch@notes.cc.sunysb.edu (T.D. Glotch).
[1] Now at Stony Brook University, Stony Brook, NY 11794, USA.

0019-1035/$ – see front matter
doi:10.1016/j.icarus.2007.07.002

2. Background

2.1. Phyllosilicates on Mars

As discussed by Bell (1996), phyllosilicates have been detected in several martian meteorites (termed the SNC meteorites) indicating that these minerals once formed on Mars. Trieman et al. (1993) identified iddingsite (a mixture of ferrihydrite and smectite clay) in the Lafayette meteorite, while Gooding and Meunow (1986), Gooding et al. (1991), and Gooding (1992) discussed the possible identification of illite/smectite mixed layer clays in the EETA79001 and Nahkla meteorites.

Until the discovery of phyllosilicates by the European Space Agency's Observatoire pour la Minéralogie, l'Eau, les Glaces, et l'Activité (OMEGA) VNIR imaging spectrometer (Bibring et al., 2005; Poulet et al., 2005; Mustard et al., 2006), in the Mawrth Vallis and Nilli Fossae regions of Mars, the presence of phyllosilicates on Mars at measurable quantities from remote sensing observations had been the subject of debate. Early evidence from VNIR telescopic and spacecraft observations showed only weak OH^- spectral features (Singer et al., 1979; McCord et al., 1982; Murchie et al., 1993; Bell et al., 1997) that could be interpreted as due to phyllosilicates. Particu-

lar emphasis was placed on the search for phyllosilicates in the martian bright regions and atmospheric dust—an effort which is summarized in detail by Hamilton et al. (2005). Early analysis of Mariner 9 Infrared Interferometer Spectrometer (IRIS) TIR spectra indicated that the composition of the dust could be modeled as montmorillonite (Hunt et al., 1973; Aronson and Emslie, 1975) or a combination of basalt and montmorillonite (Toon et al., 1977). More recent work has shown that palagonite, an amorphous weathering product of basaltic glass is a better match to the visible spectrum of the martian dust than crystalline phyllosilicates (Roush et al., 1993; Clancy et al., 1995) although it is not a good match to the TIR spectrum (Hamilton and Morris, 2003). From analysis of Mars Global Surveyor (MGS) Thermal Emission Spectrometer (TES) data, Hamilton et al. (2005) conclude that phyllosilicates are not a likely component of the martian dust.

There has also been some debate on the existence of phyllosilicates in the dark, less-dusty regions of Mars, as measured by TES. Initial TES results showed that the dark regions of Mars could be divided into two main surface types—basalt (surface Type 1; ST1) and basaltic andesite (surface Type 2; ST2) (Bandfield et al., 2000)—and that although some phyllosilicates are often present in linear deconvolution models of TES spectra, their presence does not dominate any particular geographic region of Mars (Bandfield, 2002). Wyatt and McSween (2002) showed that although a basaltic andesite mineralogy was still the best numerical fit to the TES ST2 surface shape, replacing primary volcanic glass with secondary phyllosilicate minerals also yielded an acceptable model fit. Thus, ST2 could also be interpreted as an altered basalt. Michalski et al. (2005, 2006) thoroughly investigated the spectral and crystal chemical properties of several phyllosilicates and concluded that, based on TES data, there was no unambiguous evidence for their presence in martian low albedo regions, and that poorly crystalline aluminosilicates may be more likely (e.g., Rogers and Christensen, 2007). This is in agreement with a search for phyllosilicates in TES data that concluded they are unlikely to be distributed globally (Ruff, 2003).

2.2. *Phyllosilicates in the Solar System and extrasolar disks*

The literature regarding aqueous alteration, and specifically phyllosilicate mineralogy of chondritic meteorites is vast, and demonstrates that phyllosilicate minerals are important components of these meteorites and their parent bodies. Carbonaceous chondrites show evidence of aqueous alteration in the form of phyllosilicate mineralogy ranging from pervasive to trace. Detailed reviews are given by Zolensky and McSween (1988), Buseck and Hua (1993), Rubin (1997), and Brearley (2006). CI chondrites, the most hydrated of the carbonaceous chondrites, contain serpentine and saponite within their matrices (Tomeoka and Buseck, 1988; Buseck and Hua, 1993). The phyllosilicate alteration phases of CM chondrites, on the other hand, are composed mostly of various serpentines (Barber, 1981; Richarson, 1981; MacKinnon, 1982; Zolensky et al., 1993; Lauretta et al., 2000; Hanowski and Brearley, 2001; Zega and Buseck, 2003), although cronstedtite is also observed, and accounts for much of the matrix (Tomeoka and Buseck, 1982, 1985; Buseck and Hua, 1993; Zega et al., 2003). CR chondrites tend to be less altered than CI or CM chondrites, although there are some exceptions. The phyllosilicates that are present—primarily Al-rich chlorite, and Mg-poor saponite and serpentine—are finer grained than is generally seen in other meteorites (Weisberg and Prinz, 1991; Weisberg et al., 1993; Buseck and Hua, 1993; Abreu and Brearley, 2005).

In general, aqueous alteration has affected the CO and CV chondrites to a limited extent. There are, however, some exceptions. Tomeoka and Busek (1990) found that the Mokia CV carbonaceous chondrite contains Fe-rich saponite, Na-rich phlogopite, and serpentine. This particular phyllosilicate assemblage differs considerably from phyllosilicates found in CI and CM chondrites, suggesting aqueous alteration of the parent bodies under differing conditions (Tomeoka and Buseck, 1990). The presence of fine-grained serpentine and chlorites has been reported in several CO chondrites (Ikeda, 1983; Keller and Buseck, 1990; Brearley, 1993; Itoh and Tomeoka, 2001). Finally, some unequilibrated ordinary chondrites also show evidence for aqueous alteration in the form of phyllosilicates (Hutchinson et al., 1987, 1998; Alexander et al., 1989; Grossman et al., 2000, 2002).

The extensive evidence for aqueous alteration in the carbonaceous chondrites has fueled efforts to identify alteration products in interplanetary dust particles (IDPs) and several types of asteroids to which they might be related. Most spectroscopic studies of asteroids have utilized the ultraviolet/visible (UVVIS) and VNIR portion of the spectrum. Numerous studies have indicated the presence of phyllosilicates on both main belt and outer belt asteroids (Lebofsky, 1978, 1980; Lebofsky et al., 1990; Vilas and Gaffey, 1989; King et al., 1992; Vilas et al., 1993; Vilas, 1994). Fewer studies have focused on the TIR to study asteroids, although that may change with acquisition of more data from the Spitzer Space Telescope, which launched in 2003. Recent Spitzer Infrared Spectrograph (IRS) observations of the Deep Impact encounter with Comet 9P/Tempel 1 indicated the presence of nontronite (Lisse et al., 2006, 2007). In addition, Spitzer IRS observations of Trojan asteroids in the TIR have indicated that they are composed of fine-grained silicates (Emery et al., 2006). The best spectral matches for these asteroids are the CO3 chondrites, which contain some phyllosilicates. At smaller scales, Reach et al. (2003) find that a significant component of a hydrated silicate (likely montmorillonite) is needed to fit the TIR (5–16 μm) spectral shape of the dust particles composing the zodiacal light observed by the ISOCAM instrument on the Infrared Space Observatory. This indicates that the parent bodies of the zodiacal light particles likely formed in the inner Solar System, where temperatures and pressures were high.

The zodiacal light is analogous to exozodiacal light which is responsible for most of the observed emission from other planetary systems and debris disks. Perhaps the most-studied disk is that surrounding the star β Pictoris. There have been numerous observations of β Pic in the infrared spectral region (Telesco et al., 1988; Chini et al., 1991; Telesco and Knacke, 1991; Aitken et al., 1993; Knacke et al., 1993; Lagage and Pantin,

1994; Harvey et al., 1996; Reach et al., 2003) in addition to theoretical investigations have tried to determine the composition of the dust (Artymowicz et al., 1989; Li and Greenberg, 1998). It is apparent that there are crystalline silicates in the dust surrounding β Pic, but the composition is unknown, and improved optical constants are needed to determine this (Li and Greenberg, 1998; Reach et al., 2003). Other dust disks have also been observed. D'Alessio et al. (2005) used IRS observations of CoKu Tau/4, and modeled amorphous/glassy olivine and pyroxene as the primary dust components. No crystalline silicates (either anhydrous or hydrous) were modeled. Bowey and Adamson (2002), on the other hand, found that the TIR emission spectrum of young stellar objects (YSO's) in the Taurus molecular cloud could be fit using a small ($\leqslant$10%) component of a hydrous silicate such as montmorillonite or talc. The improved optical constants of phyllosilicate minerals presented in this work should help to identify the crystalline silicate phases around β Pic and other dust disks surrounding nearby stars.

3. Methods

3.1. Sample descriptions

Details of the phyllosilicate minerals studied in this work are shown in Table 1. The minerals include aluminous, magnesian, and ferruginous phyllosilicates from the dioctahedral smectite, trioctahedral smectite, illite, kaolinite, and serpentine mineral groups. Seven of the 10 minerals used for this study are Clay Minerals Society source or special clays. These samples—nontronite, montmorillonite, beidellite, hectorite, kaolinite, illite, and illite–smectite mixed layer in a 60/40 ratio—as well as samples of saponite, halloysite, and serpentine from other sources were loaned to us by J. Michalski. Samples were originally prepared for studies by Michalski et al. (2005, 2006). The samples were placed in distilled water and centrifuged, and suspended fraction was then iteratively decanted and centrifuged again until the desired size fraction was attained. The final sample was then allowed to dry in air before analysis. X-ray characterizations of air dried and ethylene glycol-treated samples were performed on oriented powder slide mounts according to the method of Moore and Reynolds (1997) which allowed Michalski et al. (2005, 2006) to identify both expandable and non-expandable layers. The major element chemistry of the Clay Mineral Society source clays (kaolinite, hectorite, and montmorillonite) was determined by Mermut and Cano (2001). The saponite, beidellite, nontronite, and serpentine samples were characterized by Eberl et al. (1982), Post et al. (1997), Keeling et al. (2000), and Piatek (1997), respectively. The structural formulae for illite, illite–smectite, and halloysite are given by Michalski et al. (2006), and are shown here in Table 1. Each of these samples, except for the serpentine, which was also ground to a fine powder, are <2.0 or <0.2 μm size fractions that were pressed into pure pellets with mirror-like surfaces.

The smectites examined in this study were previously K-saturated to facilitate precise X-ray characterization. This process replaces the interlayer Ca^{2+} and Na^{2+} cations with K^{+} cations. Because the interlayer cations are weakly bound, the absorptions due to their presence are manifested mainly at wavenumbers less than 130 cm^{-1} (Farmer, 1974). Interlayer cations, though, can also have an affect on the bound water in molecules, and the water ν_2 band has been observed to vary in position from 1629–1640 cm^{-1} in montmorillonite with various substituted interlayer cations (Bishop et al., 1994). In general, the effect of K-saturation on the spectra presented here is minimal.

3.2. Collection and processing of spectra

Mid-infrared (100–2000 cm^{-1}; 5–100 μm) reflectance spectra were acquired at 2 cm^{-1} spectral sampling on Caltech's Nicolet Magna 860 Fourier Transform Infrared (FTIR) spectrometer equipped with a Perkin–Elmer micro-Fresnel reflection accessory with incidence and reflection angles of 20°. A schematic diagram of the reflectance accessory is shown in Fig. 1. An aluminum-coated front surface mirror was used as the reflectance standard and was assumed to have a reflectance of one. Samples were placed in a sample chamber purged of

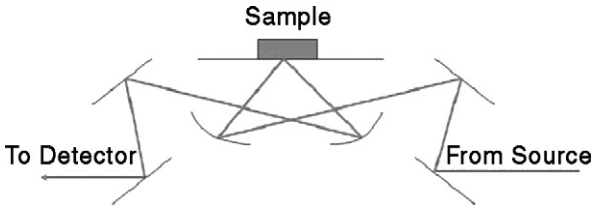

Fig. 1. Schematic diagram of the Perkin–Elmer reflectance accessory used for this study. Incidence and reflection angles are 20°.

Table 1
Data for phyllosilicates examined in this study (adapted from Michalski et al., 2006)

Source	Sample	Structural formula	Origin
CMS	SWy-1	$(Fe_{0.21}Al_{1.51}Mg_{0.27}Ti_{0.01})(Al_{0.01}Si_{3.99})O_{10}(OH)_2$	Chester County, PA, USA
CMS	SBId-1	$(Fe^{3+}{}_{0.10}Al_{1.79}Mg_{0.05}Ti_{0.05})(Al_{0.23}Si_{3.77})O_{10}(OH)_2$	Idaho, USA
CMS	NAu-1	$(Al_{0.15}Fe_{1.84}Mg_{0.02})(Al_{0.51}Si_{3.49})O_{10}(OH)_2$	Uley Mine, South Australia
CMS	SHCa-1	$(Li_{0.70}Mg_{2.30}Ti_{0.01})(Fe_{0.03}Al_{0.09}Si_{3.88})O_{10}(OH)_2$	San Bernardino County, CA, USA
D. E.	SpNv-1	$(Li_{0.09}Mg_{2.72}Fe^{3+}{}_{0.03}Al_{0.07})(Al_{0.04}Si_{3.96})O_{10}(OH)_2$	Southern Nevada, USA
CMS	IMt-1	$Mg_{0.04}Ca_{0.03}K_{0.87}(Al_{1.45}Fe^{3+}{}_{0.38}Fe^{2+}{}_{0.03}Mg_{0.22}Ti_{0.03})(Si_{3.37}Al_{0.62})O_{10}(OH)_2$	Silver Hill, MT, USA
CMS	ISMt-1	$Mg_{0.03}Ca_{0.1}K_{0.42}(Al_{1.68}Fe^{3+}{}_{0.08}Fe^{2+}{}_{0.01}Mg_{0.23}Ti_{0.01})(Si_{3.54}Al_{0.46})O_{10}(OH)_2$	Mancos Shale, USA
CMS	KGa-1a	$(Al_{1.94}Ti_{0.05}Fe_{0.01})(Si_{1.93}Al_{0.07})O_5(OH)_4$	Washington County, GA, USA
Ward's	HWw-1	$Ca_{0.01}Na_{0.02}(Al_{1.95}Fe_{0.05})(Si_{1.96}Al_{0.04})O_5(OH)_4$	Bedford, IN, USA
Burminco	BUR-1690	$(Mg_{2.81}Fe_{0.35})(Si_{1.87}Al_{0.07})O_5(OH)_4$	Mariposa County, CA, USA

CO_2 gas and H_2O vapor and spectra from two separate spectral regions were acquired for each sample. The viewing geometries for each set of spectra were identical. Mid-IR spectra were acquired from 400–4000 cm^{-1} using a KBr beamsplitter and an uncooled deuterated triglycine sulfate (DTGS) pyroelectric detector with a KBr window. A total of 512 scans were averaged to produce each spectrum. Roush et al. (1991) point out that the assumption of single reflections from pellet surfaces is likely not accurate at shorter wavelengths. For this reason, spectra are analyzed only out to 2000 cm^{-1}. Far-IR spectra were acquired from 100–600 cm^{-1} for each sample using a Nicolet Solid Substrate beamsplitter and an uncooled DTGS detector with a polyethylene window. Due to the lower signal to noise ratio (SNR) at long wavelengths, we averaged 1024 scans to produce each far-IR spectrum. Mid and Far-IR spectra of each sample were joined together near 500 cm^{-1}. Occasionally, samples had mid and far-IR spectra with slightly different spectral contrasts, perhaps due to measurement of different parts of the pellet. Differences in spectral contrast were commonly lower than 1% reflectance and never higher than 3%. In these cases, the far-IR spectrum was multiplicatively scaled to exhibit the same spectral contrast as the mid-IR spectrum.

3.3. Modeling of optical constants

To model the optical constants of the phyllosilicate minerals selected for this study, we make use of dispersion theory in combination with a Fresnel reflectance model using a non-linear least squares optimization routine. Mineral spectra are iteratively fit with a modeled spectrum produced using dispersion and Fresnel equations. When the best fit is achieved, the optical constants are determined.

Dispersion theory is a mathematical formulation that represents the vibration of a crystal lattice as the sum of the vibrations of two or more harmonic oscillators. Each vibrational mode in a mineral creates a moving dipole moment, which in turn produces the radiation that is measured in an infrared spectrum. Each model oscillator is defined by three parameters: ν, $4\pi\rho$, and γ, which represent the center frequency of the oscillation, the band strength, and damping coefficient, respectively. An additional term, ε_0, is the high frequency dielectric constant, which is a bulk mineral property rather than an oscillator-dependent property and should be equal to n^2_{vis} measured in the visible part of the spectrum (Roush et al., 1991). Dispersion equations vary slightly in the literature (e.g., Spitzer and Kleinman, 1961; Onari et al., 1977; Roush et al., 1991; Esposito et al., 2000), but we adopt the formulation of Spitzer and Kleinman (1961), which is expressed in wavenumber space rather than wavelength space.

In the Spitzer and Kleinman (1961) formulation of the dispersion equations, n and k are related to the dispersion parameters via the following equations:

$$n^2 - k^2 = \varepsilon_0 + \sum_j \frac{4\pi\rho_j \nu_j^2(\nu_j^2 - \nu^2)}{(\nu_j^2 - \nu^2)^2 + (\gamma_j^2 \nu_j^2 \nu^2)}, \tag{1}$$

$$nk = \sum_j \frac{4\pi\rho_j \nu_j^2(\gamma_j \nu_j \nu)}{(\nu_j^2 - \nu^2)^2 + (\gamma_j^2 \nu_j^2 \nu^2)}, \tag{2}$$

where n is the real index of refraction, k is the imaginary index of refraction, and j represents the jth oscillator. The input parameters (ν_j, $4\pi\rho_j$, γ_j, and ε_0) are iteratively adjusted to solve for values of n and k which, when used as inputs into the Fresnel equations for non-normal incidence, produce a modeled spectrum that has the lowest RMS error compared to the measured spectrum. The total reflectance for non-normal incidence is described as follows:

$$R_T = \frac{R_\perp^2 + R_\parallel^2}{2}, \tag{3}$$

where

$$R_\parallel^2 = \frac{(\cos\theta - u)^2 + \nu^2}{(\cos\theta + u)^2 + \nu^2}, \tag{4}$$

$$R_\perp^2 = \frac{[(n^2 - k^2)\cos\theta - u]^2 + (2nk\cos\theta - \nu)^2}{[(n^2 - k^2)\cos\theta + u]^2 + (2nk\cos\theta + \nu)^2}, \tag{5}$$

$$u = \left(\frac{n^2 - k^2 - \sin^2\theta + [(n^2 - k^2 - \sin^2\theta)^2 + 4n^2k^2]^{1/2}}{2}\right)^{1/2}, \tag{6}$$

$$\nu = \left(\frac{-(n^2 - k^2 - \sin^2\theta) + [(n^2 - k^2 - \sin^2\theta)^2 + 4n^2k^2]^{1/2}}{2}\right)^{1/2}, \tag{7}$$

and θ is the angle of incident radiation measured from the surface normal (20° for our spectrometer setup). $R_\perp$ and $R_\parallel$ (vector components perpendicular and parallel to the plane of incidence) are amplitudes, and must be squared to get the fractional intensities, which are the measured parameters.

Non-linear least squares optimization is used to solve for the best-fitting dispersion parameters. Reasonable guesses for the dispersion parameters are entered as inputs, and the routine returns optimized parameters. Following the method of Roush et al. (1991), we first placed oscillators at positions of major restrahlen bands and then added additional oscillators as necessary to improve the quality of the fit. Our model treats each point in the measured spectrum equally. Although the major vibrational bands occur in the 100–1200 cm^{-1} region, the 1200–2000 cm^{-1} region is critical for correctly determining the value of ε_0.

Roush et al. (1991) estimated the errors for their optical constants by providing several values of ε_0 for each set of dispersion parameters and observing the resultant change in the optical constants. For our purposes, we let ε_0 vary with the other dispersion parameters until an optimized solution is achieved.

A successful dispersion analysis meets the following requirements: (1) the measured and modeled spectra agree within reasonable estimates of the experimental error, (2) the number of oscillators used in the analysis is the minimum that the data require, (3) the dispersion parameters are uniquely determined by fitting the modeled spectrum to the measured, and (4) all of the dispersion parameters have positive values (Spitzer and Kleinman, 1961; Roush et al., 1991).

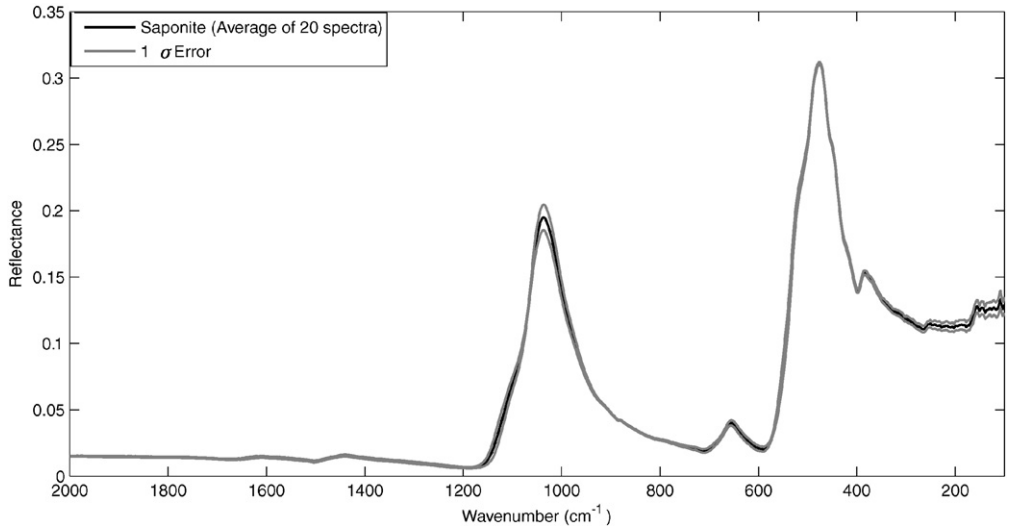

Fig. 2. Average saponite SpNv-1 spectrum and the 1σ error from 20 measurements acquired over 4 days. The maximum error is 0.0097 in reflectance, which is equal to ~3% of the maximum spectral contrast. The error over most of the spectral range is $\ll 1\%$.

4. Results

4.1. Estimates of measurement error

To asses the error associated with our laboratory reflectance measurements, we measured one sample (saponite SpNv-1) 20 times over 4 days. Each measurement was made after acquisition of a separate background spectrum. The average spectrum and associated 1σ errors are shown in Fig. 2. Errors are greatest at ~1050 cm^{-1} and at wavenumbers <300 cm^{-1}. The maximum error is 0.0097 in reflectance at 1030 cm^{-1}, which corresponds to about 3% of the maximum spectral contrast of the spectrum. Over much of the spectrum, the error is $\ll 1\%$. These results show that there is great reproducibility of sample spectra with our spectrometer setup and lend confidence to the quality of the measured spectra as well as the accuracy of the derived optical constants.

4.2. Comparison of emissivity and reflectance spectra

We have acquired reflectance spectra of 10 pressed pellet phyllosilicate samples. Comparison of these reflectance spectra to emissivity spectra acquired by Michalski et al. (2005, 2006) of similar pressed pellets shows them to be generally consistent, although some differences are evident (Fig. 3). For purposes of direct comparison, the reflectance spectra were inverted and multiplicatively scaled to have similar spectral contrast to the emissivity spectra. Optical constants described in Section 4.3 were derived from the unscaled laboratory reflectance spectra. Assuming specular reflection, reflectance spectra can be converted to emissivity spectra via Kirchhoff's law $\varepsilon = 1 - R - T$, where ε is emissivity, R is reflectance, and T is the transmittance. For a thick sample, the transmittance is zero, so the emissivity is $1 - R$. Laboratory transmission measurements of several clay pellets confirms the assumption that the transmittance is ~0% over the wavelength range measured. The emissivity spectra were acquired by Michalski et al. (2005, 2006) from 300–1400 cm^{-1}, while reflectance spectra acquired at Caltech span 100–2000 cm^{-1}. While reflectance and emission spectra of all samples show the same major restrahlen bands indicative of Si–O stretching modes (700–1200 cm^{-1}) Si–O bending modes (150–600 cm^{-1}), and O–H bending modes (600–950 cm^{-1}) (Farmer, 1974), some differences between the spectra are immediately apparent. Reflectance and emissivity spectra of beidellite and kaolinite display different relative intensities between the Si–O stretching vibrations at and the Si–O bending modes (Figs. 3b, 3i). Reflectance and emissivity spectra of montmorillonite, hectorite, illite, illite-smectite, and kaolinite have different intensities in the OH-bending region from 600–950 cm^{-1}. Differences may be due to slightly different pellet preparation techniques or slight changes in the water content of the minerals over time. Despite the differences, the overall agreement between the reflectance and emissivity spectra is good and the optical constants derived from these spectra would be similar.

4.3. Optical constants of phyllosilicates

Here we show the measured and modeled spectra for each of the minerals discussed, along with the values of n and k derived from dispersion analysis. All measured and modeled spectra as well as derived values of n and k can be accessed at http://www.ms.cc.sunysb.edu/~tglotch/optical_constants.htm or by contacting the author.

4.3.1. Dioctahedral smectites

The measured and modeled spectra, along with the derived values of n and k for the dioctahedral smectites montmorillonite, beidellite, and nontronite are shown in Figs. 4, 5, and 6. The dispersion parameters used to model n and k are given in Table 2.

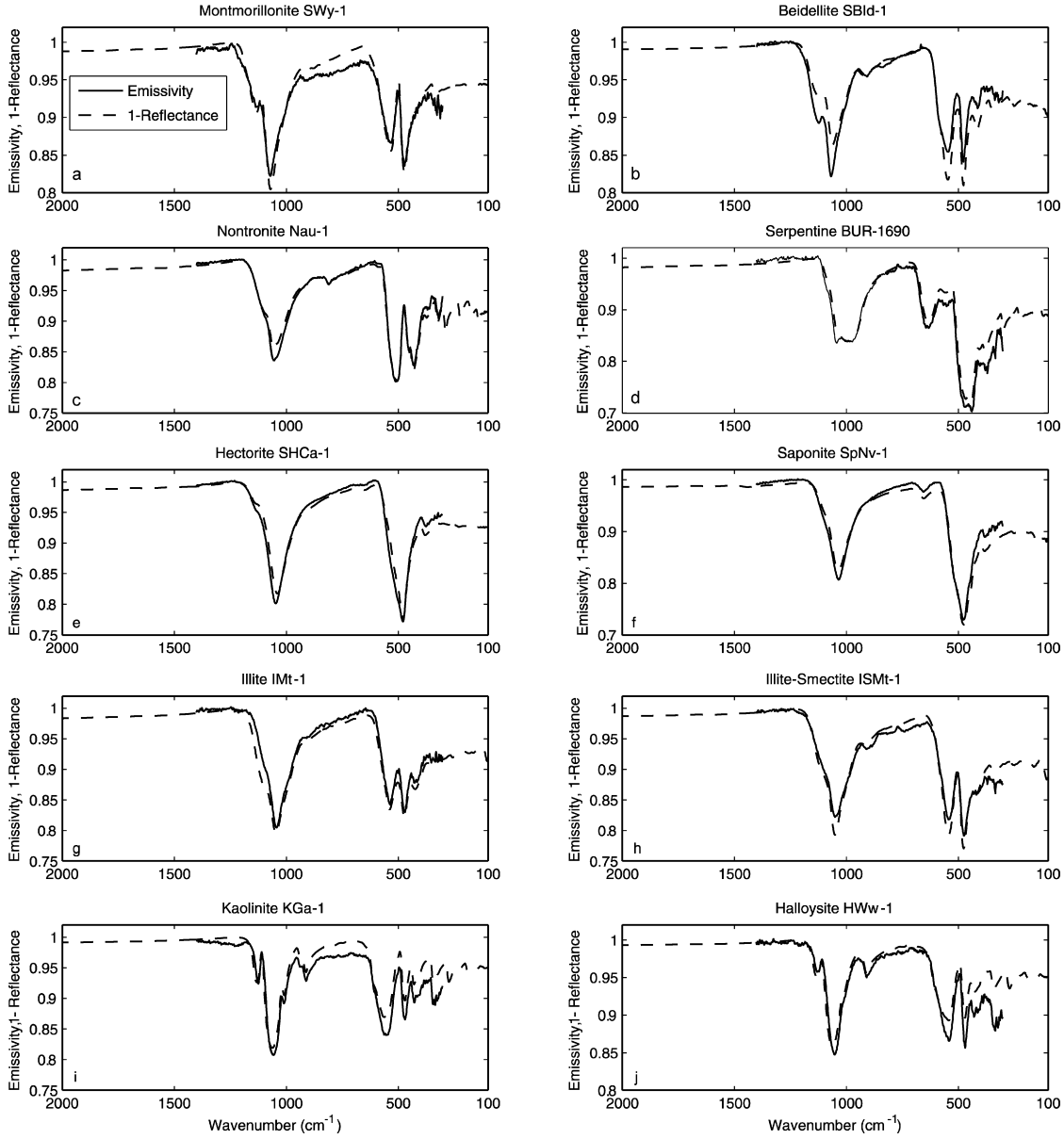

Fig. 3. Comparison of reflectance spectra acquired for this study with emissivity spectra acquired by Michalski et al. (2005, 2006). Reflectance spectra were inverted to emissivity via Kirchoff's law and multiplicatively scaled to the spectral contrast of the emissivity spectra. (a) Montmorillonite SWy-1. (b) Beidellite SBId-1. (c) Nontronite NAu-1. (d) Serpentine BUR-1690. (e) Hectorite SHCa-1. (f) Saponite SPNv-1. (g) Illite IMt-1. (h) Illite–smectite interlayered 60/40 ISMt-1. (i) Kaolinite KGa-1. (j) Halloysite HWw-1.

4.3.2. *Trioctahedral smectites*

The measured and modeled spectra, along with the derived values of n and k for the trioctahedral smectites hectorite and saponite are shown in Figs. 7 and 8. The dispersion parameters used to model n and k for these minerals are given in Table 3.

4.3.3. *Illite group*

The spectra, along with the derived values of n and k for the illite group minerals illite and illite–smectite are shown in Figs. 9 and 10. The dispersion parameters used to model n and k for these minerals are given in Table 4.

4.3.4. *Kaolinite group*

The spectra, along with the derived values of n and k for the kaolinite group minerals kaolinite and halloysite are shown in Figs. 11 and 12. The dispersion parameters used to model n and k for these minerals are given in Table 5.

4.3.5. *Serpentite group*

The measured and modeled spectra and the derived values of n and k for serpentine are shown in Fig. 13. The dispersion parameters used to model n and k for serpentine are given in Table 6.

5. Discussion

5.1. *Comparison to previous studies*

Four of the samples for which we have modeled optical constants have been modeled previously in the literature at similar

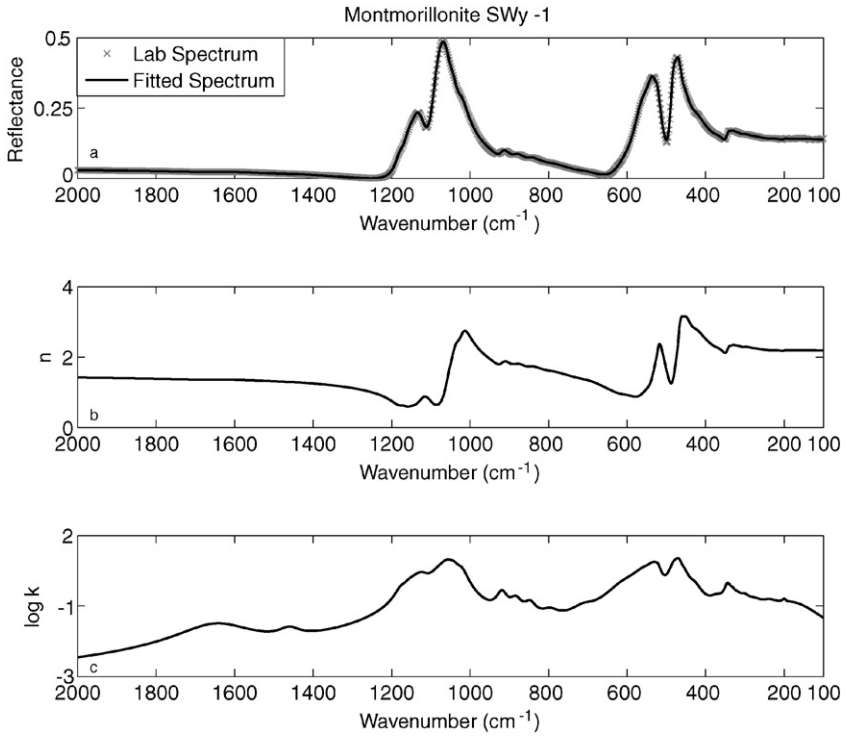

Fig. 4. Reflectance spectrum and optical constants for montmorillonite SWy-1 from 100–2000 cm^{-1}. (a) Measured and modeled reflectance spectrum. (b) Real index of refraction. (c) Imaginary index of refraction.

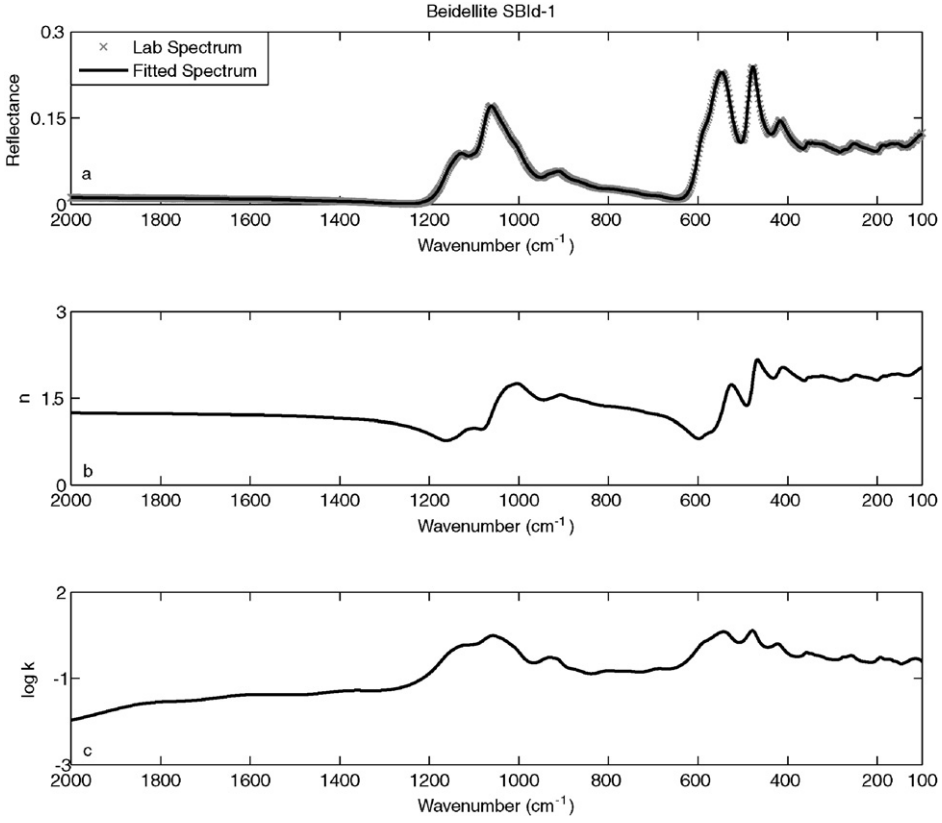

Fig. 5. Reflectance spectrum and optical constants for beidellite SBId-1 from 100–2000 cm^{-1}. (a) Measured and modeled reflectance spectrum. (b) Real index of refraction. (c) Imaginary index of refraction.

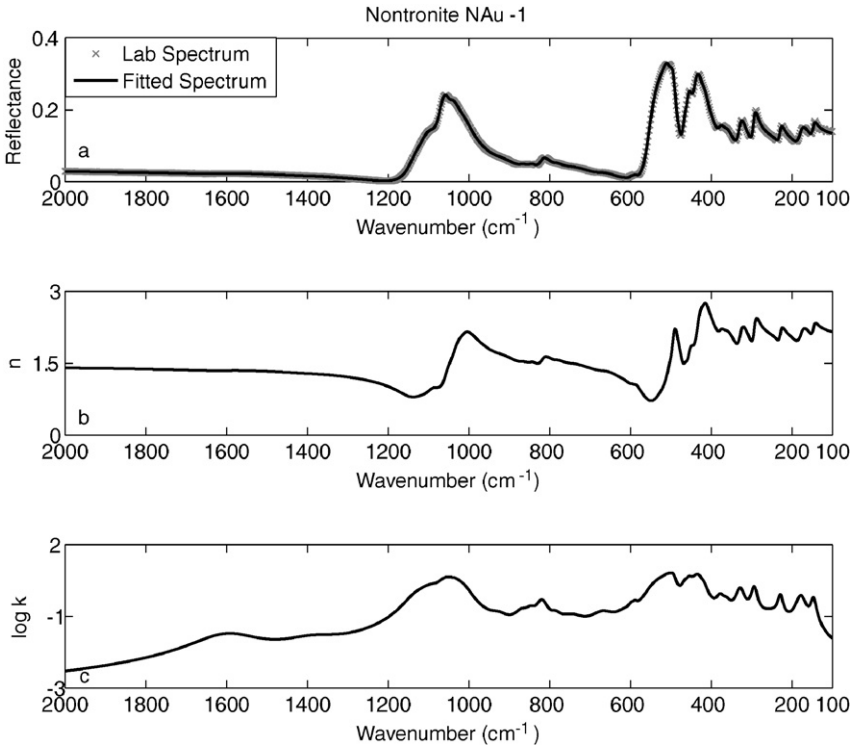

Fig. 6. Reflectance spectrum and optical constants for nontronite NAu-1 from 100–2000 cm^{-1}. (a) Measured and modeled reflectance spectrum. (b) Real index of refraction. (c) Imaginary index of refraction.

wavelengths, although our work extends further into the far-IR than most previous studies. The following sections detail the similarities and differences between our work and that of previous authors for the minerals montmorillonite, serpentine, saponite, and kaolinite.

5.1.1. Montmorillonite

Fig. 14 shows the optical constants of montmorillonite, serpentine, saponite, and kaolinite derived in this work compared to optical constants derived for these minerals in previous studies. The optical constants of montmorillonite have been previously determined by several authors (Toon et al., 1977; Koike and Shibai, 1990; Roush et al., 1991; Esposito et al., 2000). Koike and Shibai (1990) measured the extinction coefficients for montmorillonite and serpentine from 7–400 cm^{-1}, and then modeled the optical constants assuming spherical particle shapes, which is likely to lead to errors in the reported values, as phyllosilicates have platy crystal habits. For this reason, we do not consider their work here. Toon et al. (1977) determined the optical constants of two montmorillonite samples from 250–2000 cm^{-1}. In Figs. 14a and 14b, we show the optical constants determined for their sample 219b, which is most chemically similar to the Clay Mineral Society sample SWy-1 used in this work. Roush et al. (1991) determined the optical constants of montmorillonite from 400–2000 cm^{-1} at 4 cm^{-1} spectral sampling, and Esposito et al. determined the optical constants of a similar sample from 400–2500 cm^{-1} at 2 cm^{-1} spectral sampling. As can be seen in Figs. 14a and 14b, the optical constants of montmorillonite determined in this work and by other authors (Toon et al., 1977; Roush et al., 1991; Esposito et al., 2000) are in good agreement.

Although there is good agreement between the optical constants for montmorillonite derived in this and other work, there is some difference in the dispersion parameters used to model the optical constants. Roush et al. (1991) use 15 oscillators, and an ε_0 value of 1.4050 to model the optical constants, while Esposito et al. (2000) use only 13 oscillators and an ε_0 value of 1.928. In this work, we use a total of 30 oscillators, and an ε_0 value of 2.2933 to model the optical constants of montmorillonite. In order to conduct a successful dispersion analysis, one must minimize the number of oscillators used to correctly describe the data. Thus, the use of more oscillators by our model is not in and of itself an improvement. Our data extend to 100 cm^{-1}, as opposed to 400 cm^{-1} for the Roush et al. (1991) data and Esposito et al. (2000). We used 9 oscillators to model the optical constants from 100–400 cm^{-1}, which was outside of the spectral range modeled by the other authors. Our data are also low noise (Fig. 2) due to long scan times, which allowed us to model weak bands, and weak features on the shoulders of strong bands that were not previously modeled. Finally, our non-linear least squares optimization model significantly reduced the time required to model many oscillators as compared to previous iterative approaches. This increases the feasibility of using additional oscillators to more accurately describe the data.

Fig. 15 shows the %RMS reflectance error between the measured and modeled spectra as a function of the number of oscillators used in model. Unsurprisingly, the error decreases with the number of oscillators used, and starts to flattens out (but is

Table 2
Oscillator parameters for the dioctahedral smectites

Montmorillonite SWy-1			Beidellite SBId-1			Nontronite NAu-1		
$\varepsilon_0 = 2.2933$			$\varepsilon_0 = 1.7558$			$\varepsilon_0 = 2.1730$		
ν (cm^{-1})[a]	γ	$4\pi\rho$	ν (cm^{-1})	γ	$4\pi\rho$	ν (cm^{-1})	γ	$4\pi\rho$
189	0.6774	0.3008	116	0.6035	0.5912	146	0.0914	0.1121
200	0.0455	0.0059	156	0.0825	0.0099	177	0.1378	0.1959
239	0.2204	0.0576	173	0.1821	0.0820	228	0.0529	0.0673
277	0.1604	0.0461	193	0.1126	0.0491	257	0.3370	0.1276
302	0.1042	0.0487	229	0.3036	0.1307	292	0.0480	0.1222
320	0.0684	0.0242	258	0.1116	0.0625	327	0.0632	0.1373
332	0.0522	0.0315	276	0.0709	0.0182	363	0.0703	0.0434
344	0.0473	0.0599	294	0.0617	0.0056	377	0.0521	0.0478
372	0.1034	0.0414	304	0.0207	0.0008	417	0.0382	0.0513
430	0.0855	0.1209	337	0.2465	0.1985	431	0.0654	0.3903
454	0.0541	0.1977	346	0.0209	0.0016	453	0.0430	0.1010
467	0.0374	0.3400	357	0.0324	0.0093	465	0.0256	0.0154
478	0.0325	0.0693	420	0.0661	0.0730	493	0.0297	0.1086
521	0.0323	0.1338	451	0.2978	0.3097	503	0.0553	0.1329
531	0.0454	0.1305	475	0.0479	0.1655	522	0.1074	0.1253
551	0.0923	0.1373	536	0.0740	0.2052	588	0.0222	0.0027
601	0.1633	0.1025	557	0.0859	0.0382	597	0.0289	0.0038
711	0.0824	0.0085	585	0.0604	0.0219	618	0.0577	0.0041
797	0.0578	0.0059	693	0.1081	0.0176	669	0.0962	0.0200
848	0.0359	0.0094	755	0.0837	0.0094	748	0.0959	0.0180
884	0.0352	0.0138	803	0.0990	0.0194	785	0.0325	0.0043
919	0.0290	0.0204	874	0.0695	0.0114	818	0.0353	0.0247
1021	0.0314	0.1350	913	0.0285	0.0067	847	0.0282	0.0056
1041	0.0290	0.1526	933	0.0581	0.0319	868	0.0447	0.0106
1056	0.0248	0.0689	1008	0.0350	0.0186	927	0.0537	0.0074
1120	0.0396	0.0438	1033	0.0508	0.0739	1013	0.0453	0.0778
1152	0.0299	0.0048	1056	0.0445	0.0674	1034	0.0413	0.1120
1174	0.0228	0.0029	1101	0.0395	0.0126	1054	0.0292	0.0365
1460	0.0380	0.0010	1124	0.0416	0.0196	1092	0.0484	0.0368
1647	0.1083	0.0080	1149	0.0483	0.0111	1125	0.0584	0.0179
			1381	0.1484	0.0084	1386	0.1170	0.0038
			1602	0.1929	0.0133	1599	0.1058	0.0077
			1828	0.1310	0.0045			

[a] In this and following tables, ν is the center frequency of the oscillator, $4\pi\rho$ is the band strength, γ is the damping coefficient, and ε_0 is the high frequency dielectric constant.

still decreasing) as the final number of oscillators used is approached. We make use of the derived RMS error as well as qualitative evaluation of the measured and modeled spectra to determine the optimal number of oscillators.

5.1.2. Serpentine

Figs. 14c and 14d show the optical constants of serpentine determined in this work, and by Mooney and Knacke (1985) and Roush et al. (1991). There is good agreement between the optical constants derived in this work and by Roush et al. (1991), while the values determined by Mooney and Knacke (1985) are less consistent. This may be due to one or more of several factors. The optical constants derived from both this work and that of Roush et al. (1991) were determined from spectra of pressed pellets of serpentine fines. The optical constants derived by Mooney and Knacke (1985) were determined from spectra acquired of a polished serpentine-rich rock which contained 94% serpentine flakes in addition to 5% fine-grained magnetite and 1% dolomite. The presence of some magnetite in the sample of Mooney and Knacke (1985) could account for some of the observed difference in the 400–200 cm^{-1} spectral region, where iron oxides have fundamental Fe–O stretching vibrations. Mooney and Knacke (1985) did not publish the dispersion parameters that they used for their work, but Roush et al. (1991) used 10 oscillators and an ε_0 value of 1.4000 to model the serpentine optical constants. For this work, we used 29 oscillators and an ε_0 value of 2.0581. Once again, 9 oscillators were used to model the optical constants from 100–400 cm^{-1}, a spectral range which was not modeled by Roush et al. (1991). Difficulty in modeling the structure of the large band centered at $\sim$1000 cm^{-1} prompted us to use several oscillators to achieve a desirable fit.

5.1.3. Saponite

Roush et al. (1991) modeled the optical constants of saponite using 8 oscillators and an ε_0 value of 1.3134. We expanded the model of saponite optical constants using 27 oscillators and an ε_0 value of 1.8403. A comparison of the derived optical constants of saponite is shown in Figs. 14e and 14f, and some immediate differences are apparent. Roush et al. (1991) model only one hydration feature at 1620 cm^{-1}. Our saponite spectrum (Fig. 6) shows two distinct features at 1440 and

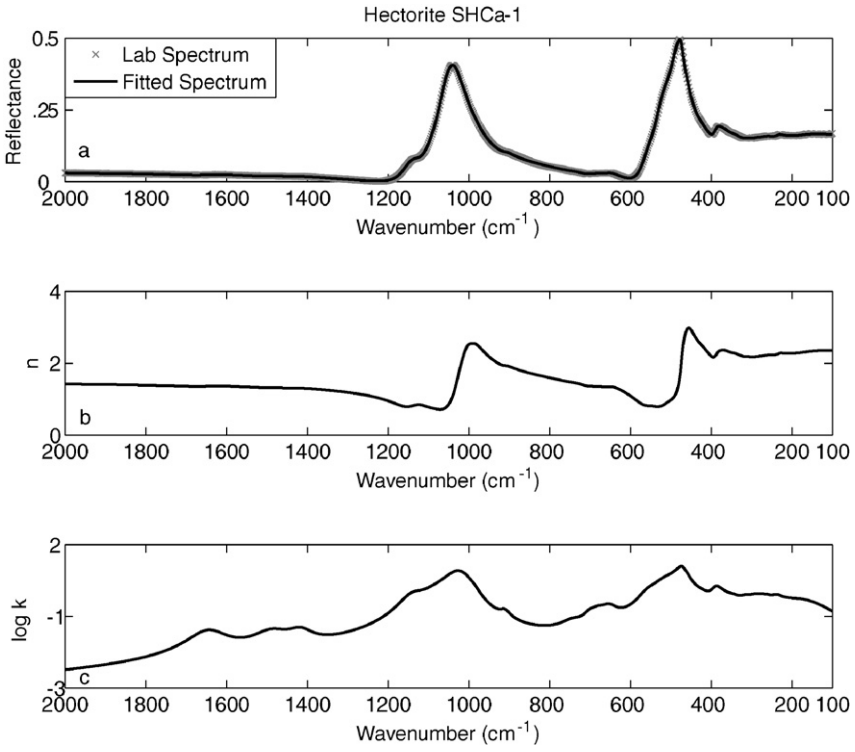

Fig. 7. Reflectance spectrum and optical constants for hectorite SHCa-1 from 100–2000 cm^{-1}. (a) Measured and modeled reflectance spectrum. (b) Real index of refraction. (c) Imaginary index of refraction.

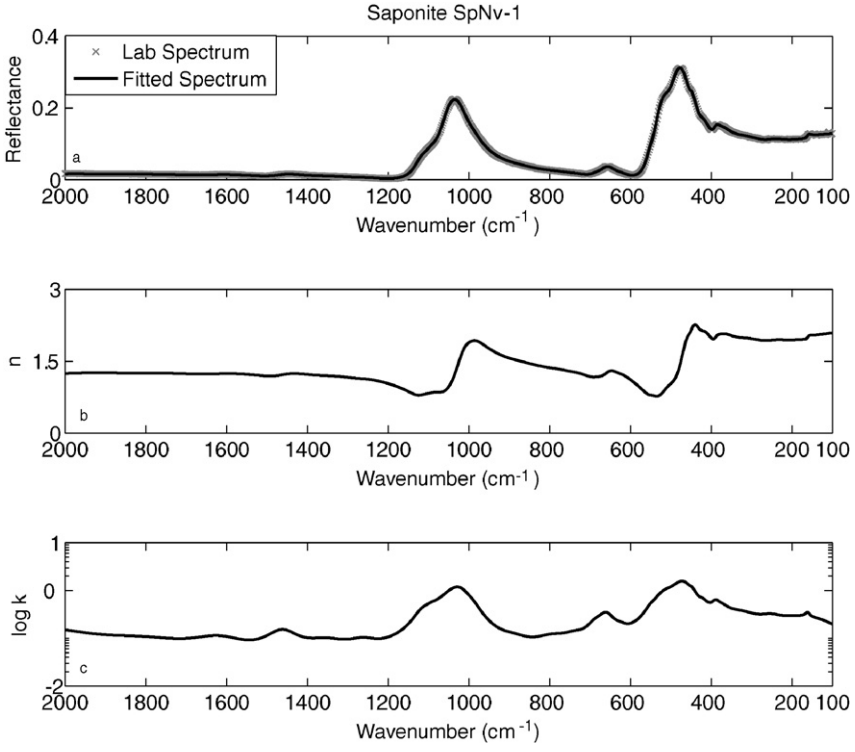

Fig. 8. Reflectance spectrum and optical constants for saponite SpNv-1 from 100–2000 cm^{-1}. (a) Measured and modeled reflectance spectrum. (b) Real index of refraction. (c) Imaginary index of refraction.

1610 cm^{-1}. The 1440 cm^{-1} feature is unlikely to be due to hydration, but there is another possibility. Ammonium (NH_4^+) is a common substitution ion in several types of minerals, including sulfates (Chourabi and Fripiat, 1981) and smectite clays (Altaner et al., 1988). Ammonium substitution could account for the presence of the 1440 cm^{-1} seen in the saponite spec-

Table 3
Oscillator parameters for trioctahedral smectites

Hectorite SHCa-1			Saponite SpNv-1		
$\varepsilon_0 = 2.2680$			$\varepsilon_0 = 1.8403$		
ν (cm^{-1})	γ	$4\pi\rho$	ν (cm^{-1})	γ	$4\pi\rho$
196	0.8577	1.0116	161	0.0805	0.0225
212	0.0963	0.0048	226	1.5493	1.2785
232	0.0303	0.0019	253	0.1156	0.0174
239	0.1799	0.1161	340	0.3438	0.1901
261	0.0698	0.0125	376	0.1028	0.0663
272	0.1223	0.0550	389	0.0478	0.0297
290	0.1352	0.0810	420	0.0655	0.0416
314	0.1226	0.0663	446	0.0488	0.0753
347	0.1326	0.0998	466	0.0855	0.3419
373	0.0948	0.0868	479	0.2278	0.2752
386	0.0656	0.0938	512	0.0612	0.0211
431	0.1331	0.1516	620	0.0594	0.0054
464	0.0711	0.6149	658	0.0744	0.0403
471	0.0281	0.0914	689	0.0677	0.0101
506	0.1160	0.1207	741	0.1099	0.0122
551	0.0950	0.0323	797	0.1121	0.0151
654	0.0713	0.0230	861	0.0712	0.0041
681	0.0484	0.0078	881	0.0131	0.0006
700	0.0422	0.0054	917	0.0227	0.0012
745	0.0772	0.0059	986	0.0383	0.0133
911	0.0317	0.0068	1013	0.0469	0.0646
990	0.0398	0.0648	1030	0.0571	0.1172
1008	0.0344	0.1184	1096	0.0686	0.0282
1023	0.0408	0.1721	1306	0.2043	0.0295
1085	0.0662	0.0213	1459	0.0638	0.0107
1132	0.0582	0.0273	1624	0.0702	0.0067
1418	0.0448	0.0029	1927	0.4488	0.0553
1488	0.0642	0.0046			
1645	0.0598	0.0054			

Table 4
Oscillator parameters for the illite group

Illite IMt-1			Illite/smectite ISMt-1		
$\varepsilon_0 = 2.2010$			$\varepsilon_0 = 1.8470$		
ν (cm^{-1})	γ	$4\pi\rho$	ν (cm^{-1})	γ	$4\pi\rho$
109	0.2652	0.3316	116	0.3146	0.3322
133	0.1414	0.0218	168	0.1401	0.0405
168	0.0982	0.0156	191	0.1622	0.0424
193	0.1814	0.0630	218	0.5184	0.2284
254	0.2335	0.0836	243	0.0365	0.0014
263	0.0478	0.0104	261	0.1178	0.0410
299	0.1140	0.0267	295	0.0339	0.0011
333	0.1513	0.0859	300	0.2593	0.0929
355	0.0727	0.0419	341	0.1170	0.0845
372	0.0455	0.0130	357	0.0296	0.0037
396	0.0160	0.0035	376	0.1150	0.0294
420	0.0537	0.0367	421	0.0889	0.1236
432	0.0913	0.2088	449	0.0976	0.0543
471	0.0674	0.3513	474	0.0637	0.2880
522	0.1293	0.3976	530	0.0702	0.1758
532	0.0528	0.0502	547	0.0849	0.0989
572	0.1038	0.0433	582	0.0797	0.0323
635	0.0668	0.0061	619	0.0781	0.0137
688	0.0987	0.0199	692	0.1422	0.0299
753	0.0751	0.0166	753	0.0609	0.0087
778	0.0257	0.0023	824	0.1443	0.0327
799	0.0199	0.0025	920	0.0494	0.0260
830	0.0387	0.0052	1011	0.0564	0.1093
876	0.0357	0.0030	1040	0.0458	0.1067
914	0.0238	0.0098	1087	0.0395	0.0127
1003	0.0422	0.1258	1115	0.0575	0.0254
1030	0.0463	0.2089	1422	0.1991	0.0176
1087	0.0472	0.0319	1621	0.0869	0.0055
1119	0.0617	0.0167	1839	0.2461	0.0124
1169	0.0297	0.0013			
1432	0.0620	0.0016			
1623	0.2007	0.0119			

trum. This additional oscillator in the high wavenumber region of the spectrum has the effect of raising the value of k (Fig. 14f) compared to that determined by Roush et al. (1991).

5.1.4. Kaolinite

The kaolinite optical constants derived in this work are compared to those previously derived by Roush et al. (1991) in Figs. 14g and 14h. The comparison between the two is quite good, although as in previous cases, we require more oscillators (to model subtle features) and a higher value of ε_0 to model the spectrum. Roush et al. (1991) use 15 oscillators and an ε_0 value of 1.4400 to model the optical constants of kaolinite, while we find that 32 oscillators and an ε_0 value of 2.2221 are required to achieve the best model fit.

5.1.5. Discrepancies in the value of ε_0

The modeled values of ε_0 should be equal to the square of the visible index of refraction (Roush et al., 1991). Although our derived values of ε_0 are closer to the measured n^2_{vis} than those derived by previous work (Mooney and Knacke, 1985; Roush et al., 1991; Esposito et al., 2000), for all samples except montmorillonite and hectorite, they generally fall below the values calculated from measured n_{vis}. As briefly discussed by Roush et al. (1991), this is consistent with a decreasing value of n throughout the VNIR portion of the spectrum, past 2000 cm^{-1} until n approaches the initial dispersion region near 1200–1300 cm^{-1}. It is possible that our derived values of ε_0 are larger than those from previous work because we cover a larger portion of the infrared spectrum.

5.2. Implications for TIR remote sensing of phyllosilicates

As shown in Section 4.2, the reflectance spectra from which these optical constants are derived are consistent with emissivity spectra previously acquired by Michalski et al. (2005, 2006) over the wavelength range for which they overlap. Therefore, the optical constants derived here will be applicable to studies which make use of emissivity spectra of Mars, asteroids, other airless bodies, interplanetary and interstellar dust, and protoplanetary disks.

The role of volume scattering and its affect on the TIR spectra of fine particulates has been discussed extensively (Lyon, 1964; Hunt and Vincent, 1968; Vincent and Hunt, 1968; Aronson and Emslie, 1973; Salisbury and Eastes, 1985; Salisbury and Wald, 1992; Wald and Salisbury, 1995) and optical constants are a critical component of any radiative transfer model that attempts to correctly model the scattering of small particulates in emissivity or reflectance spectra (e.g., Hapke, 1981, 1984, 1986, 1993a, 1993b, 1996a, 1996b; Moersch and Chris-

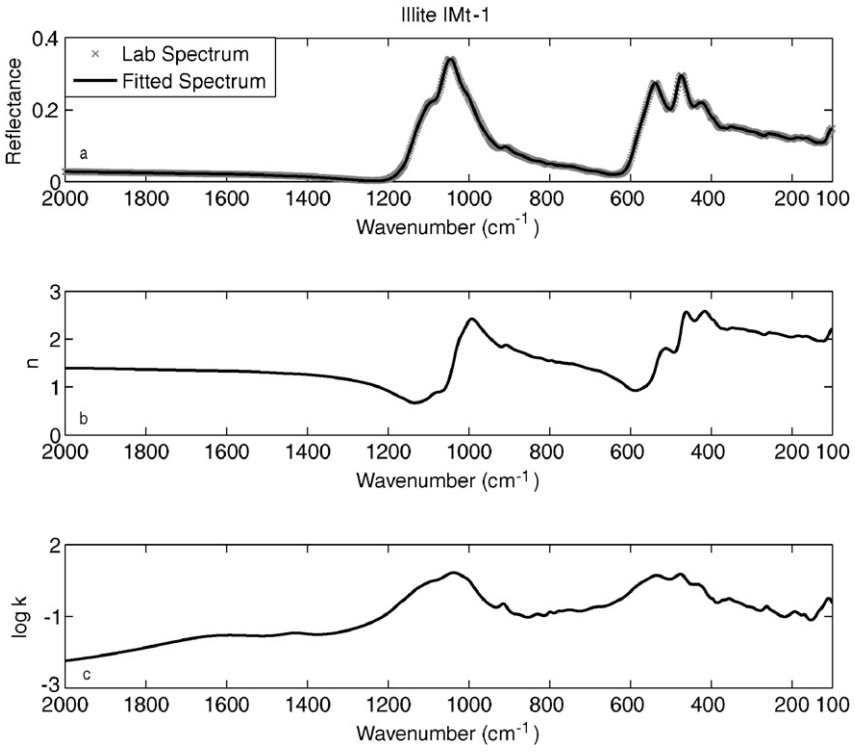

Fig. 9. Reflectance spectrum and optical constants for illite IMt-1 from 100–2000 cm^{-1}. (a) Measured and modeled reflectance spectrum. (b) Real index of refraction. (c) Imaginary index of refraction.

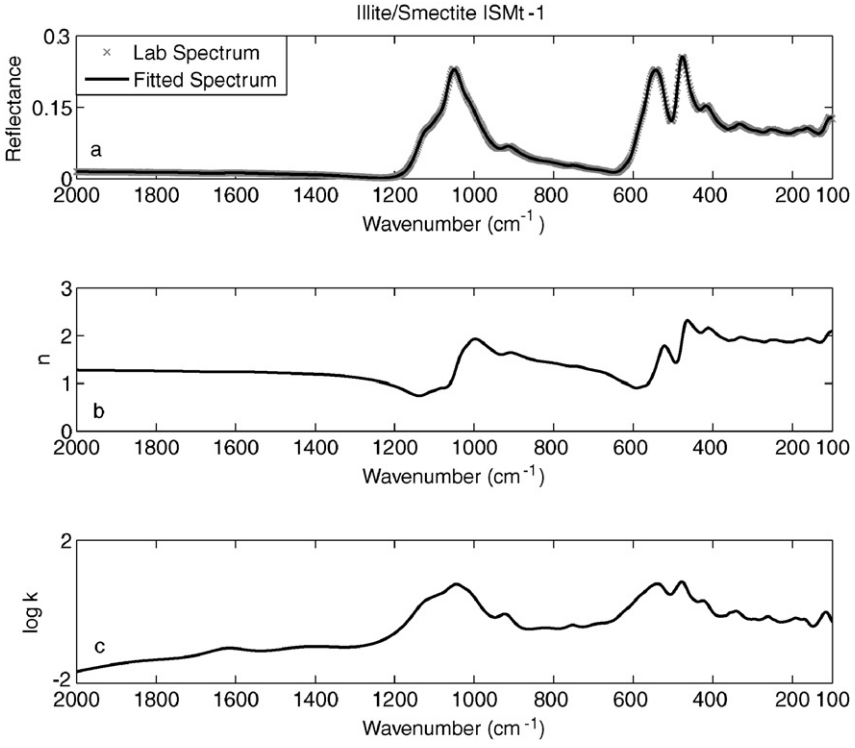

Fig. 10. Reflectance spectrum and optical constants for illite–smectite interlayered 60/40 ISMt-1 from 100–2000 cm^{-1}. (a) Measured and modeled reflectance spectrum. (b) Real index of refraction. (c) Imaginary index of refraction.

tensen, 1995; Mustard and Hayes, 1997; Pitman et al., 2005). Much of the surface of Mars is covered by a finely particulate dust that has an estimated grain size of <10 μm (Bandfield and Smith, 2003) or even <5 μm (Pollack et al., 1979). In addition, spectra of the surfaces of the Moon and asteroids are dominated by fine-grained components (e.g., Pieters et al., 1993;

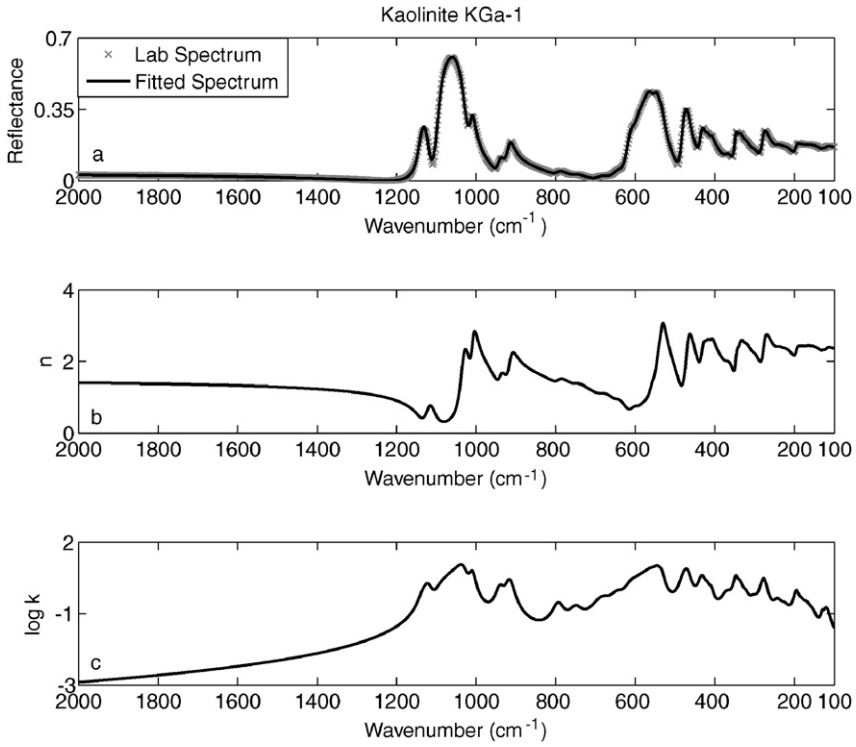

Fig. 11. Reflectance spectrum and optical constants for kaolinite KGa-1 from 100–2000 cm^{-1}. (a) Measured and modeled reflectance spectrum. (b) Real index of refraction. (c) Imaginary index of refraction.

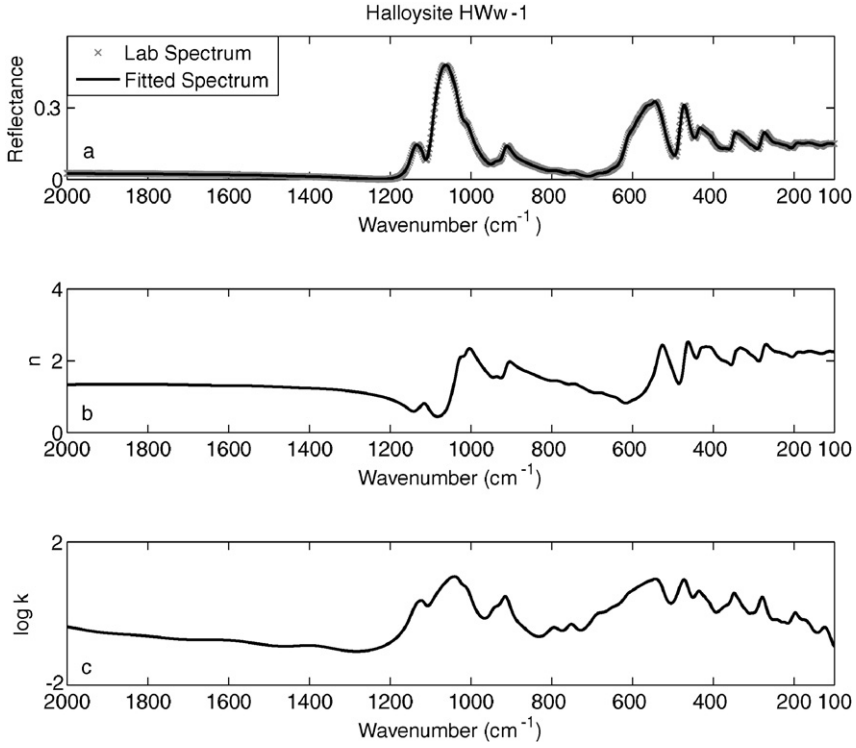

Fig. 12. Reflectance spectrum and optical constants for halloysite HWw-1 from 100–2000 cm^{-1}. (a) Measured and modeled reflectance spectrum. (b) Real index of refraction. (c) Imaginary index of refraction.

Emery et al., 2006). Although phyllosilicates are not expected to form on the Moon, some evidence for their presence near the south polar region has been presented (Vilas et al., 1998). More robust detections have been made of phyllosilicates occurring on asteroids (Lebofsky, 1978, 1980; Lebofsky et al., 1990; Vilas and Gaffey, 1989; King et al., 1992; Vilas et al., 1993,

Table 5
Oscillator parameters for kaolinite group

Kaolinite KGa-1			Halloysite HWw-1		
$\varepsilon_0 = 2.2221$			$\varepsilon_0 = 1.9318$		
ν (cm^{-1})	γ	$4\pi\rho$	ν (cm^{-1})	γ	$4\pi\rho$
120	0.1608	0.0930	124	0.2736	0.1909
130	0.0381	0.0065	149	0.0337	0.0052
156	0.1191	0.0301	157	0.0682	0.0149
169	0.1262	0.0693	168	0.1090	0.0592
184	0.1186	0.0765	182	0.1289	0.0644
195	0.0687	0.1019	197	0.1060	0.1190
226	0.1340	0.0643	223	0.1064	0.0335
243	0.0886	0.0577	242	0.1289	0.0746
276	0.0617	0.2710	277	0.0747	0.2385
303	0.0753	0.0447	303	0.0820	0.0356
323	0.0595	0.0597	322	0.0738	0.0544
337	0.0488	0.1388	336	0.0565	0.0854
347	0.0295	0.0911	347	0.0450	0.1160
370	0.0832	0.0921	371	0.1059	0.1209
409	0.0299	0.0413	410	0.0483	0.0594
420	0.0361	0.0654	420	0.0343	0.0326
431	0.0394	0.1664	433	0.0532	0.1879
469	0.0417	0.3291	468	0.0438	0.3208
534	0.0280	0.1734	534	0.0490	0.3044
543	0.0332	0.1866	556	0.0801	0.1903
558	0.0516	0.1540	592	0.1059	0.1025
581	0.0694	0.0660	648	0.0488	0.0127
604	0.0455	0.0215	683	0.0682	0.0298
644	0.0557	0.0212	751	0.0381	0.0108
683	0.0727	0.0311	795	0.0555	0.0164
750	0.0452	0.0120	873	0.0610	0.0152
793	0.0357	0.0161	912	0.0284	0.0643
915	0.0230	0.0749	940	0.0270	0.0175
939	0.0223	0.0304	1010	0.0257	0.0745
1008	0.0146	0.0916	1034	0.0327	0.2000
1033	0.0229	0.1977	1123	0.0264	0.0172
1120	0.0190	0.0149	1408	0.0839	0.0060
			1600	0.1219	0.0120
			1828	0.1356	0.0093

Table 6
Oscillator parameters for serpentine

Serpentine BUR-1690		
$\varepsilon_0 = 2.0581$		
ν (cm^{-1})	γ	$4\pi\rho$
107	0.1552	0.0274
127	0.1115	0.0637
201	0.0720	0.0050
228	0.0524	0.0350
233	0.0301	0.0122
245	0.9494	0.4505
303	0.0533	0.0750
373	0.1598	0.1509
385	0.0627	0.1141
405	0.0517	0.0803
438	0.0621	0.4029
461	0.0813	0.2937
482	0.0668	0.0648
501	0.0387	0.0146
556	0.0970	0.0928
615	0.0790	0.1121
637	0.0928	0.1031
780	0.1765	0.0197
937	0.0238	0.0157
949	0.0220	0.0256
959	0.0226	0.0349
970	0.0253	0.0370
983	0.0289	0.0357
997	0.0335	0.0369
1014	0.0380	0.0302
1036	0.0464	0.0325
1079	0.0381	0.0078
1311	0.1903	0.0115
1600	0.2525	0.0200

1994). Because most phyllosilicates, and all clay minerals, are inherently finely crystalline, it may be necessary to more quantitatively model the spectral properties of these minerals in TIR spectra. Although current scattering models cannot account for all the spectral features associated with volume scattering in fine particulates, advances have been made, such as the incorporation of Mie theory into scattering models (Moersch and Christensen, 1995; Mustard and Hayes, 1997). However, it is likely that future models will have to better account for non-spherical particle shapes and packing density (Pitman et al., 2005). Future improvements in radiative transfer scattering models, coupled with the use of optical constants generated in this and other studies will allow researchers to quantitatively model the effects of mineralogy and particle size for interplanetary and interstellar dust, protoplanetary disks, and planetary surfaces which are dominated by finely particulate materials.

6. Conclusions

We have acquired mid-infrared (100–2000 cm^{-1}) reflectance spectra of 10 phyllosilicate samples, including montmorillonite, beidellite, nontronite, hectorite, saponite, illite, an illite-smectite interlayered clay consisting of 60% illite and 40% smectite, kaolinite, halloysite, and serpentite. From these spectra, we have determined the real and imaginary indices of refraction using classical Lorentz–Lorenz dispersion theory. The derived optical constants of montmorillonite, serpentine, saponite, and kaolinite compare favorably with the optical constants previously derived by other authors for these minerals (e.g., Toon et al., 1977; Mooney and Knacke, 1985; Roush et al., 1991; Esposito et al., 2000) over the regions in which they overlap. The high spectral resolution (2 cm^{-1} sampling) of our data has allowed us to identify weak bands in the spectra that have not previously been modeled, and the increased spectral range has allowed us to generate robust optical constants of these clay minerals in the far infrared (400–100 cm^{-1})—a region for which the optical constants of minerals have not commonly been determined. The optical constants for the clay minerals described here may aid in future work such as determining the mineralogy of interplanetary and interstellar dust, the fine-grained surfaces of airless bodies, protoplanetary disks surrounding young nearby stars, and the search for phyllosilicate minerals using on Mars using the mid-IR portion of the spectrum.

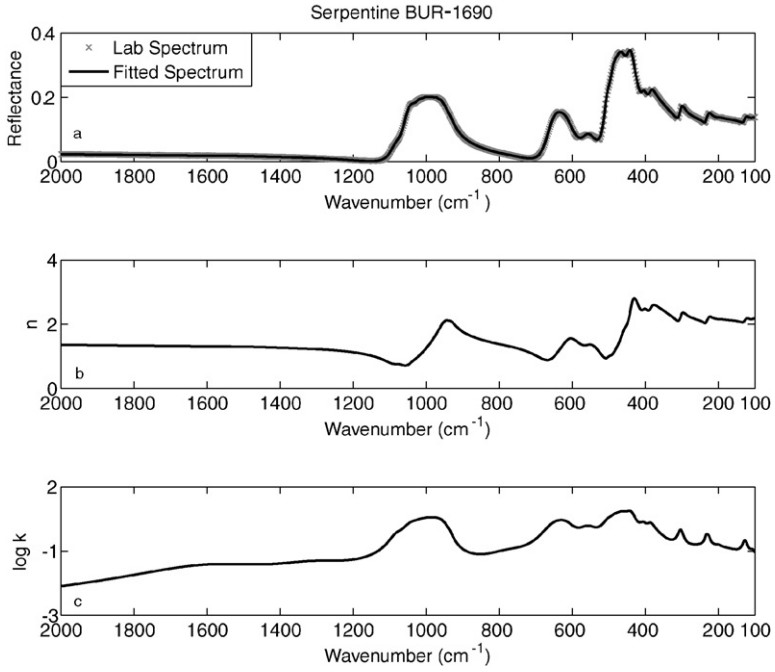

Fig. 13. Reflectance spectrum and optical constants for serpentine BUR-1690 from 100–2000 cm^{-1}. (a) Measured and modeled reflectance spectrum. (b) Real index of refraction. (c) Imaginary index of refraction.

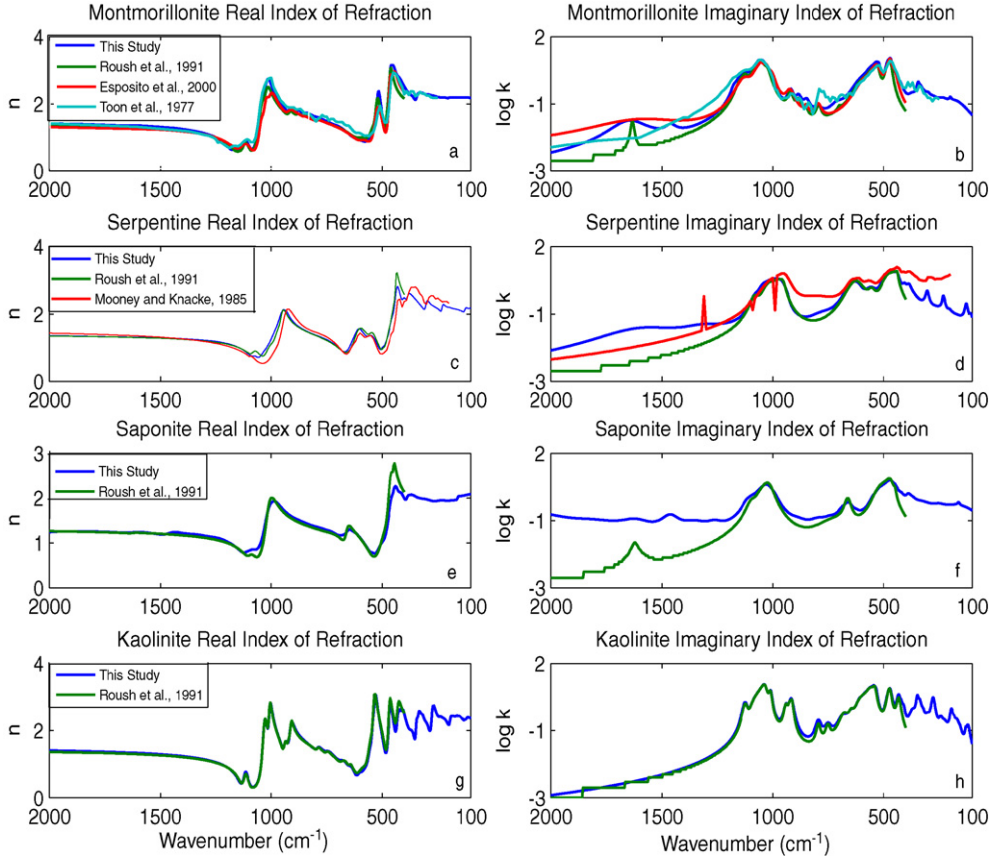

Fig. 14. Comparison of optical constants derived in this study to those derived in other studies. (a) The real index of refraction of montmorillonite derived in this study and by Roush et al. (1991), Esposito et al. (2000), and Toon et al. (1977). (b) The imaginary index of refraction of montmorillonite derived in this study and by Roush et al. (1991), Esposito et al. (2000), and Toon et al. (1977). (c) The real index of refraction of serpentine derived in this study and by Roush et al. (1991) and Mooney and Knacke (1985). (d) The imaginary index of refraction of serpentine derived in this study and by Roush et al. (1991) and Mooney and Knacke (1985). (e) The real index of refraction of saponite derived in this study and by Roush et al. (1991). (f) The imaginary index of refraction of saponite derived in this study and by Roush et al. (1991). (g) The real index of refraction of kaolinite derived in this study and by Roush et al. (1991). (h) The imaginary index of refraction of kaolinite derived in this study and by Roush et al. (1991).

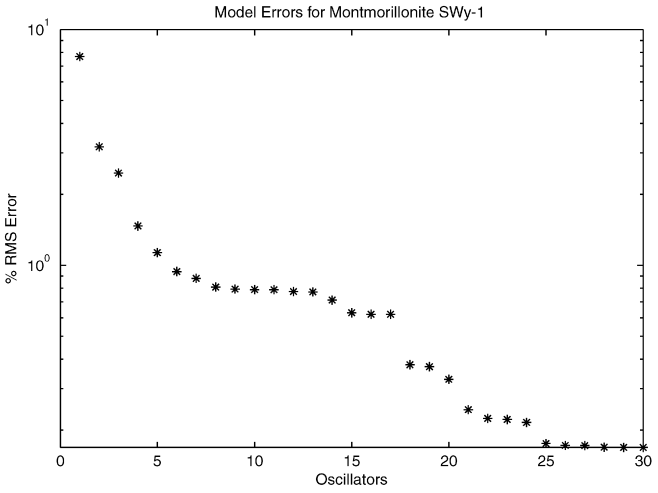

Fig. 15. Percent root mean square (%RMS) reflectance error between the modeled and measured spectra of montmorillonite SWy-1 as a function of the number of oscillators used in the model.

Acknowledgments

We thank J. Michalski for loaning well characterized phyllosilicate samples for our reflectance measurements. We also thank Ted Roush and Ed Cloutis for thorough reviews that improved the manuscript. This work was supported by the NASA Mars Fundamental Research Program.

References

Abreu, N.M., Brearley, A.J., 2005. HRTEM and EFTEM studies of phyllosilicate–organic matter associations in matrix and dark inclusions in the EET92042 CR2 carbonaceous chondrite. Lunar Planet. Sci. XXXVI. Abstract 1744 [CD-ROM].

Aitken, D.K., Moore, T.J.T., Roche, P.F., Smith, C.H., Wright, C.M., 1993. Midinfrared spectroscopy of Beta-Pictoris—Constraints on the dust grain size. Mon. Not. R. Astron. Soc. 265, L41–L43.

Alexander, C.M.O., Hutchinson, R., Barber, D.J., 1989. Origin of chondrule rims and interchondrule matrices in unequilibrated ordinary chondrites. Earth Planet. Sci. Lett. 95, 187–207.

Altaner, S.P., Fitzpatrick, J.J., Krohn, M.D., Bethke, P.M., Hayba, D.O., Goss, J.A., Brown, Z.A., 1988. Ammonium in alunites. Am. Mineral. 73, 145–152.

Aronson, J.R., Emslie, A.G., 1973. Spectral reflectance and emittance of particulate materials. 2. Application and results. Appl. Opt. 12, 2573–2584.

Aronson, J.R., Emslie, A.G., 1975. Composition of the martian dust as derived by spectroscopy from Mariner 9. J. Geophys. Res. 80, 4925–4931.

Artymowicz, P., Burrows, C., Paresce, F., 1989. The structure of the Beta Pictoris circumstellar disk from combined IRAS and coronographic observations. Astrophys. J. 337, 494–513.

Bandfield, J.L., 2002. Global mineral distributions on Mars. J. Geophys. Res. 107 (E6), doi:10.1029/2001JE001510.

Bandfield, J.L., Smith, M.D., 2003. Multiple emission angle surface–atmosphere separations of Thermal Emission Spectrometer data. Icarus 161, 47–65.

Bandfield, J.L., Hamilton, V.E., Christensen, P.R., 2000. A global view of martian surface compositions from MGS-TES. Science 287, 1626–1630.

Barber, D.J., 1981. Phyllosilicates and other layer-structured minerals in stony meteorites. Clay Miner. 20, 415–454.

Bell III, J.F., 1996. Iron sulfate, carbonate, and hydrated minerals on Mars. In: Dyar, M.D., McCammon, C., Schaefer, M.W. (Eds.), Mineral Spectroscopy: A Tribute to Roger G. Burns. Geochemical Society Special Publication 5, pp. 359–380.

Bell III, J.F., Wolff, M.J., James, P.B., Clancy, R.T., Lee, S.W., Martin, L.J., 1997. Mars surface mineralogy from the Hubble Space Telescope imaging during 1994–1995: Observations, calibration, and initial results. J. Geophys. Res. 102 (E4), 9109–9124, doi:10.1029/96JE03990.

Bibring, J.-P., Langevin, Y., Gendrin, A., Gondet, B., Poulet, F., Berthe, M., Soufflot, A., Arvidson, R., Mangold, N., Mustard, J., Drossart, P., and the OMEGA Team, 2005. Mars surface diversity as revealed by the OMEGA/Mars Express Observations. Science 307, 1576–1581.

Bishop, J.L., Pieters, C.M., Edwards, J.O., 1994. Infrared spectroscopic analyses on the nature of water in montmorillonite. Clays Clay Miner. 42, 702–716.

Bowey, J.E., Adamson, A.J., 2002. A mineralogy of extrasolar silicate dust from 10-μm spectra. Mon. Not. R. Astron. Soc. 334 (1), 94–106.

Brearley, A.J., 1993. Matrix and fine-grained rims in the unequilibrated CO3 chondrite, ALHA77307: Origins and evidence for diverse, primitive nebular dust components. Geochim. Cosmochim. Acta 57, 1521–1550.

Brearley, A.J., 2006. The action of water. In: Lauretta, D.S., McSween Jr., H.Y. (Eds.), Meteorites and the Early Solar System II. Univ. of Arizona, Tuscon, pp. 587–624.

Busek, P.R., Hua, X., 1993. Matrices of carbonaceous chondrite meteorites. Annu. Rev. Earth Planet. Sci. 21, 255–305.

Chini, R., Krügel, E., Shustov, B., Tutukov, A., Kreysa, E., 1991. Dust disks around Vega-type stars. Astron. Astrophys. 252, 220–228.

Chourabi, B., Fripiat, J.J., 1981. Determination of tetrahedral substitutions and interlayer surface heterogeneity from vibrational spectra of ammonium in smectites. Clays Clay Miner. 29, 260–268.

Clancy, R.T., Lee, S.W., Gladstone, G.R., McMillan, W.W., Roush, T., 1995. A new model for Mars atmospheric dust based upon analysis of ultraviolet through infrared observations from Mariner 9, Viking, and Phobos. J. Geophys. Res. 100, 5251–5264.

D'Alessio, P., and 13 colleagues, 2005. The truncated disk of CoKu Tau/4. Astrophys. J. 621, 461–472.

Eberl, D.D., Jones, B.F., Khoury, H.N., 1982. Mixed-layer kerolite/stevensite from the Amargosa Desert, Nevada. Clays Clay Miner. 30, 321–326.

Emery, J.P., Cruikshank, D.P., Van Cleve, J., 2006. Thermal emission spectroscopy (5.2–38 μm) of three Trojan asteroids with the Spitzer Space Telescope: Detection of fine-grained silicates. Icarus 182, 496–512.

Esposito, F., Colangeli, L., Palomba, E., 2000. Infrared reflectance spectroscopy of martian analogs. J. Geophys. Res. 105, 17643–17654.

Farmer, V.C., 1974. The layer silicates. In: Farmer, V.C. (Ed.), The Infrared Spectra of Minerals. Mineralogical Society, London, pp. 331–363.

Gooding, J.L., 1992. Soil mineralogy and chemistry on Mars: Possible clues from salts and clays in SNC Meteorites. Icarus 99, 28–41.

Gooding, J.L., Meunow, D.W., 1986. Martian volatiles in shergottite EETA79001: New evidence from oxidized sulfur and sulfur-rich aluminosilicates. Geochim. Cosmochim. Acta 50, 1049–1059.

Gooding, J.L., Wentworth, S.J., Zolensky, M.E., 1991. Aqueous alteration of the Nakhla meteorite. Meteoritics 26, 135–143.

Grossman, J.N., Alexander, C.M.O'D., Wang, J., Brearley, A.J., 2000. Bleached chondrules: Evidence for widespread aqueous processes on the parent asteroids of ordinary chondrites. Meteorit. Planet. Sci. 35, 467–486.

Grossman, J.N., Alexander, C.M.O., Wang, J.H., Brearley, A.J., 2002. Zoned chondrules in Semarkona: Evidence for high- and low-temperature processing. Meteorit. Planet. Sci. 37, 49–73.

Hamilton, V.E., Morris, R.V., 2003. Thermal emission spectra of altered tephras and constraints on the composition of martian dust. Lunar Planet. Sci. XXXIV. Abstract 1936.

Hamilton, V.E., McSween Jr., H.Y., Hapke, B., 2005. Mineralogy of martian atmospheric dust inferred from thermal infrared spectra of aerosols. J. Geophys. Res. 110, doi:10.1029/2005JE002501. E12006.

Hanowski, N.P., Brearley, A.J., 2001. Aqueous alteration of chondrules in the CM carbonaceous chondrites, Allan Hills 81002. Geochim. Cosmochim. Acta 65, 495–518.

Hapke, B., 1981. Bidirectional reflectance spectroscopy. 1. Theory. J. Geophys. Res. 86, 3039–3054.

Hapke, B., 1984. Bidirectional reflectance spectroscopy. 3. Correction for macroscopic roughness. Icarus 59, 41–59.

Hapke, B., 1986. Bidirectional reflectance spectroscopy. 4. The extinction coefficient and the opposition effect. Icarus 67, 264–280.

Hapke, B., 1993a. Combined theory of reflectance and emittance spectroscopy. In: Pieters, C.M., Englert, P.A. (Eds.), Remote Geochemical Analysis: Elemental and Mineralogical Composition. Cambridge Univ. Press, New York.

Hapke, B., 1993b. Theory of Emittance and Reflectance Spectroscopy. Cambridge Univ. Press, New York.

Hapke, B., 1996a. A model of radiative and conductive energy transfer in planetary regoliths. J. Geophys. Res. 101, 16817–16832.

Hapke, B., 1996b. Applications of an energy transfer model to three problems in planetary regoliths: The solid-state greenhouse, thermal beaming, and emittance spectra. J. Geophys. Res. 101, 16833–16840.

Harvey, P.M., Smith, B.J., DiFrancesco, J., Colome, C., Low, F.J., 1996. Far-infrared constraints on dust shells around Vega-like stars. Astrophys. J. 471, 973–978.

Hunt, G.R., Vincent, R.K., 1968. The behavior of spectral features in the infrared emission from particulate surfaces of various grain sizes. J. Geophys. Res. 73, 6039–6046.

Hunt, G.R., Logan, L.M., Salisbury, J.W., 1973. Mars: Components of infrared spectra and the composition of the dust cloud. Icarus 18, 459–469.

Hutchinson, R., Alexander, C.M.O.D., Barber, D.J., 1987. The Semarkona meteorite: First recorded occurrence of smectite in an ordinary chondrite, and its implications. Geochim. Cosmochim. Acta 51, 1875–1882.

Hutchinson, R., Alexander, C.M.O.D., Bridges, J.C., 1998. Elemental redistribution in Tieschitz and the origin of white matrix. Meteorit. Planet. Sci. 33, 1169–1180.

Ikeda, Y., 1983. Alteration of chondrules and matrices in the four Antarctic carbonaceous chondrites ALH77307 (C3), Y-790123 (C2), Y75293 (C2), and Y-74662 (C2). In: Proc. 8th Symp. Antarct. Met. Mem. Natl. Inst. Polar Res. vol. 30, pp. 93–108.

Itoh, S., Tomeoka, K., 2001. Phyllosilicate-bearing chondrules and clasts in the ALHA77307 CO3 chondrite: Evidence for parent-body processes. In: Antarctic Meteorites XXVI, papers presented to the 26th Symposium on Antarctic Meteorites, National Institute of Polar Research, Tokyo, pp. 47–49.

Keeling, J.L., Raven, M.D., Gates, W.P., 2000. Geology and characterization of two hydrothermal nontronites from weathered metamorphic rocks at the Uley graphite mine, south Australia. Clays Clay Mineral. 48 (5), 537–548.

Keller, L.P., Buseck, P.R., 1990. Matrix mineralogy of the Lancé CO3 carbonaceous chondrite: A transmission electron microscope study. Geochim. Cosmochim. Acta 54, 1155–1163.

King, T.V.V., Clark, R.N., Calvin, W.M., Sherman, D.M., Brown, R.H., 1992. Evidence for ammonium-bearing minerals on Ceres. Science 255, 1551–1553.

Knacke, R.F., Fajardo-Acosta, S.B., Telesco, C.M., Hackwell, J.A., Lynch, K.D., Russel, R.W., 1993. The silicates in the disk of Beta-Pictoris. Astrophys. J. 418, 440–450.

Koike, C., Shibai, H., 1990. Optical-constants of hydrous silicates from 7–400 μm. Mon. Not. R. Astron. Soc. 246, 332–336.

Lagage, P.O., Pantin, E., 1994. Dust depletion in the inner disk of Beta-Pictoris as a possible indicator of planets. Nature 369, 628–630.

Lauretta, D.S., Hua, X., Buseck, P.R., 2000. Mineralogy of fine-grained rims in the ALH81002 CM chondrite. Geochim. Cosmochim. Acta 64, 3263–3273.

Lebofsky, L.A., 1978. Asteroid 1 Ceres: Evidence for water of hydration. Mon. Not. R. Astron. Soc. 182, 17–21.

Lebofsky, L.A., 1980. Infrared reflectance spectra of asteroids: A search for water of hydration. Astron. J. 85, 573–585.

Lebofsky, L.A., Jones, T.D., Owensby, P.D., Feierberg, M.A., Consolmagno, G.J., 1990. The nature of low-albedo asteroids from 3-μm multicolor photometry. Icarus 83, 16–26.

Li, A., Greenberg, J.M., 1998. A comet dust model for the β Pictoris disk. Astron. Astrophys. 331, 291–313.

Lisse, C.M., and 16 colleagues, 2006. Spitzer spectral observations of the Deep Impact ejecta. Science 313, 635–640.

Lisse, C.M., Kraemer, K.E., Nuth III, J.A., Li, A., Joswiak, D., 2007. Comparison of the composition of the Tempel 1 ejecta to the dust in Comet C/Hale–Bopp 1995 O1 and YSO HD 100546. Icarus 187, 69–86.

Lyon, R.J.P., 1964. Evaluation of infrared spectrophotometry for compositional analysis of lunar and planetary soils. II. Rough and powdered surfaces. NASA Conf. Rep. CR-100.

MacKinnon, I.D.R., 1982. Ordered mixed-layer structures in the Mighei carbonaceous chondritic matrix. Geochim. Cosmochim. Acta 46, 479–489.

McCord, T.B., Clark, R.L., Singer, R.B., 1982. Mars: Near infrared spectral reflectance of surface regions and compositional implications. J. Geophys. Res. 87 (B4), 3021–3032.

Mermut, A.R., Cano, A.F., 2001. Baseline studies of the Clay Mineral Society source clays: Chemical analyses of major elements. Clays Clay Miner. 49 (5), 381–386.

Michalski, J.R., Kraft, M.D., Sharp, T.G., Williams, L.B., Christensen, P.R., 2005. Mineralogical constraints on the high-silica martian surface component observed by TES. Icarus 174, 161–177.

Michalski, J.R., Kraft, M.D., Sharp, T.G., Williams, L.B., Christensen, P.R., 2006. Emission spectroscopy of clay minerals and evidence for poorly crystalline aluminosilicates on Mars from Thermal Emission Spectrometer data, J. Geophys. Res. 111, doi:10.1029/2005JE002438. E03004.

Moersch, J.E., Christensen, P.R., 1995. Thermal emission from particulate surfaces: A comparison of scattering models with measured spectra. J. Geophys. Res. 100 (E4), 7465–7477.

Mooney, T., Knacke, R.F., 1985. Optical constants of chlorite and serpentine between 2.5 and 50 μm. Icarus 64, 493–502.

Moore, D.M., Reynolds Jr., R.C., 1997. X-ray Diffraction and the Identification and Analysis of Clay Minerals. Oxford Univ. Press, New York. 378 pp.

Murchie, S.L., Mustard, J., Bishop, J., Head, J., Pieters, C., Erard, S., 1993. Spatial variations in the spectral properties of bright regions on Mars. Icarus 105, 454–468.

Mustard, J.F., Hayes, J.E., 1997. Effects of hyperfine particles on reflectance spectra from 0.3 to 25 μm. Icarus 125, 145–163.

Mustard, J.F., Poulet, F., Head, J.W., Mangold, N., Bibring, J.–P., Fassett, C., Langevin, Y., Neukum, G., 2006. Ancient crust, aqueous alteration, and impact melt preserved in the Isidis Basin, Mars. Lunar Planet. Sci. XXXVII. Abstract 1683 [CD-ROM].

Onari, S., Arai, T., Kudo, K., 1977. Infrared lattice vibrations and dielectric dispersion in α-Fe_2O_3. Phys. Rev. B 16, 1717–1721.

Piatek, J.L., 1997. Vibrational spectroscopy of clay minerals: Implications for remote sensing of terrestrial planetoids. M.S. thesis, Arizona State Univ., Tempe. 75 pp.

Pieters, C.M., Fischer, E.M., Rode, O., Basu, A., 1993. Optical effects of space weathering: The role of the finest fraction. J. Geophys. Res. 98, 20817–20824.

Pitman, K.M., Wolff, M.J., Clayton, G.C., 2005. Application of modern radiative transfer tools to model laboratory quartz emissivity. J. Geophys. Res. 110, doi:10.1029/2005JE002428. E08003.

Pollack, J.B., Colburn, D.S., Flaser, F.M., Kahn, R., Carlston, C.E., Pidek, D.C., 1979. Properties and effects of dust particles suspended in the martian atmosphere. J. Geophys. Res. 84, 2929–2945.

Post, J.L., Cupp, B.L., Madsen, F.T., 1997. Beidellite and associated clays from the DeLamar Mine and Florida Mountain area, Idaho. Clays Clay Miner. 45 (2), 240–250.

Poulet, F., Bibring, J.-P., Mustard, J.F., Gendrin, A., Mangold, N., Langevin, Y., Arvidson, R.E., Gondet, B., Gomez, C., and the Omega Team, 2005. Phyllosilicates on Mars and implications for early martian climate. Nature 438, 623–627.

Reach, W.T., Morris, P., Boulanger, F., Koryo, O., 2003. The mid-infrared spectrum of the zodiacal and exozodiacal light. Icarus 164, 384–403.

Richardson, S.M., 1981. Alteration of mesostasis in chondrules and aggregates from three C2 carbonaceous chondrites. Earth Planet. Sci. Lett. 52, 67–75.

Rogers, A.D., Christensen, P.R., 2007. Surface mineralogy of martian low-albedo regions from MGS-TES data: Implications for upper crustal evolution and surface alteration. J. Geophys. Res. 112, doi:10.1029/2006JE002727. E01003.

Roush, T., Pollack, J., Orenberg, J., 1991. Derivation of midinfrared (5–25 μm) optical constants of some silicates and palagonite. Icarus 94, 191–208.

Roush, T.L., Blaney, D.L., Singer, R.B., 1993. The surface composition of Mars as inferred from spectroscopic observations. In: Pieters, C., Englert, P. (Eds.), Remote Geochemical Analysis: Elemental and Mineralogical Composition. Cambridge Univ. Press, pp. 367–393.

Rubin, A.E., 1997. Mineralogy of meteorite groups. Meteorit. Planet. Sci. 32, 231–247.

Ruff, S.W., 2003. Basaltic andesite or weathered basalt: A new assessment. In: Sixth Int. Conf. on Mars, Pasadena, CA. Abstract 3258.

Salisbury, J.W., Eastes, J.W., 1985. The effect of particle size and porosity on spectral contrast in the mid-infrared. Icarus 64, 586–588.

Salisbury, J.W., Wald, A.E., 1992. The role of volume scattering in reducing spectral contrast of restrahlen bands in spectra of powdered minerals. Icarus 96, 121–128.

Singer, R.B., McCord, T.B., Clark, R.L., Adams, J.B., Huguenin, R.L., 1979. Mars surface composition from reflectance spectroscopy: A summary. J. Geophys. Res. 84 (B14), 8415–8426.

Spitzer, W.G., Kleinman, D.A., 1961. Infrared lattice bands of quartz. Phys. Rev. 121, 1324–1335.

Telesco, C.M., Knacke, R.F., 1991. Detection of silicates in the Beta-Pictoris disk. Astrophys. J. 372, L29–L31.

Telesco, C.M., Becklin, E.E., Wolstencroft, R.D., Decher, R., 1988. Resolution of the circumstellar disk of β Pictoris at 10 and 20 μm. Nature 335, 51–53.

Tomeoka, K., Buseck, P.R., 1982. High resolution transmission electron microscopy observations of "poorly characterized phase" in the Mighei C2M carbonaceous chondrite. Meteoritics 17, 289–290.

Tomeoka, K., Buseck, P.R., 1985. Indicators of aqueous alteration in CM carbonaceous chondrites: Microtextures of a layered mineral containing Fe, S, O, and Ni. Geochim. Cosmochim. Acta 49, 2149–2163.

Tomeoka, K., Buseck, P.R., 1988. Matrix mineralogy of the Orgueil CI carbonaceous chondrite. Geochim. Cosmochim. Acta 52, 1627–1640.

Tomeoka, K., Buseck, P.R., 1990. Phyllosilicates in the Mokoia CV carbonaceous chondrite: Evidence for aqueous alteration in an oxidizing condition. Geochim. Cosmochim. Acta 54, 1745–1754.

Toon, O.B., Pollack, J.B., Sagan, C., 1977. Physical properties of the particles composing the martian dust storm of 1971–1972. Icarus 30, 663–696.

Trieman, A.H., Barrett, R.A., Gooding, J.L., 1993. Preterrestrial alteration of the Lafayette (SNC) meteorite. Meteoritics 28, 86–97.

Vilas, F., 1994. Iron alteration minerals in the visible and near-infrared spectra of low-albedo asteroids. Icarus 109, 274–283.

Vilas, F., Gaffey, M.J., 1989. Phyllosilicate absorption features in main-belt and outer-belt asteroid reflectance spectra. Science 246, 790–792.

Vilas, F.S., Larson, S.M., Sawyer, S.R., Gaffey, M.J., 1993. Ferric iron in primitive asteroids: A 0.43-μm absorption feature. Icarus 102, 225–231.

Vilas, F.S., Jarvis, K.S., Gaffey, M.J., 1994. Iron alteration minerals in the visible and near-infrared spectra of low albedo asteroids. Icarus 109, 274–283.

Vilas, F., Jensen, E., Domingue, D., McFadden, L., Coombs, C., Mendell, W., 1998. Evidence for phyllosilicates near the lunar south pole. In: Workshop on New Views of the Moon: Integrated Remotely Sensed, Geophysical, and Sample Datasets, p. 73.

Vincent, R.K., Hunt, G.R., 1968. Infrared reflectance from mat surfaces. Appl. Opt. 7, 53–58.

Wald, A.E., Salisbury, J.W., 1995. Thermal infrared directional emissivity of powdered quartz. J. Geophys. Res. 100, 24241–24250.

Weisberg, M.K., Prinz, M., 1991. Aqueous alteration in CR2 chondrites. Lunar Planet. Sci. XXII, 1483–1484.

Weisberg, M.K., Prinz, M., Clayton, R.N., Mayeda, T.K., 1993. The CR (Renazzo-type) carbonaceous chondrite group and its implications. Geochim. Cosmochim. Acta 57, 1567–1586.

Wyatt, M.B., McSween Jr., H.Y., 2002. Spectral evidence for weathered basalt as an alternative to andesite in the northern lowlands of Mars. Nature 417, 263–266.

Zega, T.J., Buseck, P.R., 2003. Fine-grained-rim mineralogy of the Cold Bokkeveld CM chondrite. Geochim. Cosmochim. Acta 67, 1711–1721.

Zega, T.J., Garvie, L.A.J., Buseck, P.R., 2003. Nanometer-scale measurements of iron oxidation states of cronstedtite from primitive meteorites. Am. Mineral. 88, 1169–1172.

Zolensky, M.E., McSween Jr., H.Y., 1988. Aqueous alteration. In: Kerridge, J.F., Matthews, M. (Eds.), Meteorites and the Early Solar System. Univ. of Arizona, Tuscon, pp. 114–143.

Zolensky, M.E., Barrett, R., Browning, L., 1993. Mineralogy and composition of matrix and chondrule rims in carbonaceous chondrites. Geochim. Cosmochim. Acta 57, 3123–3148.